American Chemical Science Journal
4(6): 828-846, 2014

SCIENCEDOMAIN *international*
www.sciencedomain.org

Heat and Mass Transfer Through a Porous Media of MHD Flow of Nanofluids with Thermal Radiation, Viscous Dissipation and Chemical Reaction Effects

Eshetu Haile[1*] and B. Shankar[1]

[1]*Department of Mathematics, Osmania University, Hyderabad 500-007, India.*

Authors' contributions

This work was carried out in collaboration between the two authors EH and BS. Author BS designed the study, wrote the protocol and wrote the first draft of the manuscript. Author EH deals with the calculation part, managed the analysis of the study and executed the program. Both authors read and approved the final manuscript.

Original Research Article

Received 25th April 2014
Accepted 5th June 2014
Published 5th July 2014

ABSTRACT

The flow problem presented in the paper is a study on boundary layer flow of a nanofluid through a porous medium subjected to a magnetic field, thermal radiation, viscous dissipation and chemical reaction effects. The effects of porosity, thermal radiation, magnetic field, viscous dissipation and chemical reaction to the flow field were thoroughly explained for various values of the governing parameters. Copper (Cu) and Alumina (Al_2O_3) water nanofluids were considered. The partial differential equations appearing in the governing equations of the problem were transformed into a couple of nonlinear ordinary differential equations with the help of similarity transformations. The transformed equations were solved numerically by the Keller Box method. For selected values of the parameters involved in the governing equations like nanofluid volume fraction $\emptyset$, the porous medium parameter K, magnetic parameter M, Eckert number Ec, Schmidt number Sc, Soret number Sr, thermal radiative parameter R and chemical reaction parameter γ, numerical results of velocity field, temperature distribution, concentration, Skin friction coefficient, Nusselt number and Sherwood number were obtained. The results were analysed and discussed with the help of graphs and tables. Comparisons with previously published works were performed and they are found in excellent agreement.

**Corresponding author: Email: eshetuhg@gmail.com, bandarishanker@yahoo.co.in;*

keywords: Heat and mass transfer; MHD flow; nanofluids; porous media; thermal radiation; viscous dissipation; chemical reaction.

1. INTRODUCTION

Nanofluids are solid-liquid composite materials consisting of solid nanoparticles or nanofibers, with sizes typically on the order of 1–100 nm, suspended in a liquid. Nanofluids are characterized by an enrichment of a base fluid like water, toluene, ethylene glycol or oil with nanoparticles in variety of types like Metals, Oxides, Carbides, Carbon, Nitrides, etc. Today nanofluid are sought to have wide range of applications in medical application, biomedical industry, detergency, power generation in nuclear reactors and more specifically in any heat removal involved industrial applications. The ongoing research ever since then has extended to utilization of nanofluids in microelectronics, fuel cells, pharmaceutical processes , hybrid-powered engines, engine cooling, vehicle thermal management, domestic refrigerator, chillers, heat exchanger, nuclear reactor coolant, grinding, machining, space technology, defence and ships, and boiler flue gas temperature reduction [1].

Choi [2] studied much on enhancing thermal conductivity of fluids with nanoparticles, developments and applications of non-Newtonian flows. Mnyusiwella [3] indicated some of the possible dangers of nanotechnology in public health and environment. A comprehensive survey of convective transport in nanofluids has been made by Buongiorno [4], who gave satisfactory explanation for the abnormal increase of thermal conductivity and viscosity relative to the base fluid. Hamada and Ismail [5] examined magnetic field effects on free convection flow of a nanofluid past a vertical semi-infinite flat plate. A study on boundary layer flow of a nanofluid past a stretching sheet with a convective boundary condition was conducted by Makinde and Aziz [6]. Recently, Ahmad [7] presented a numerical study on the Blasius and Sakiadis problems in nanofluids under isothermal condition. Kameswaran et al. [8] examined hydromagnetic nanofluid flow due to a stretching or shrinking sheet with viscous dissipation and chemical reaction effects. Khan and Pop [9] studied Boundary-layer flow of a nanofluid past a stretching sheet. Khan [10] studied the unsteady free convection boundary layer flow of a nanofluid along a stretching sheet with thermal radiation and viscous dissipation effects in the presence of a magnetic field. One of the factors affecting the flow of nanofluids is charges of the suspended nanoparticles. Nanofluids consisting of negatively charged nanoparticles suspended in aqueous Nacl solutions show significantly different velocity profiles compared to aqueous Nacl solutions containing no nanoparticles. The negatively charged nanoparticles induce an electric field and the induced electric field changes the velocity profile of the flow. The new flow phenomenon is attributed to the electrokinetic effect of charged nanoparticles that significantly increases the induced electric field strength. The streaming current due to the movement of charged nanoparticles induces an electric field and the induced electric field changes the velocity distribution of the flow [11]. Aggregation and sedimentation are also the other factors which reduce the stability of the flow of nanofluids. Nanoparticles' aggregation means that nanoparticles aggregate to form a cluster or small nanoparticle clusters aggregate to form a big cluster. Nanoparticles' sedimentation means that some nanoparticles or nanoparticle clusters settle down and finally separate out of nanofluid. Nanoparticles' aggregation and sedimentation limit its applications [12].

Earlier studies in fluid flow through a porous media have revealed the Darcy law which relates linearly the flow velocity to the pressure gradient across the porous medium. The porous medium is also characterized by its permeability which is a measure of the flow conductivity in the porous medium. Later developments in porous media led to extended

advanced models for the Darcy law such as Forchheimers equation and Brinkmans equation [13] where the former is applicable for large flow velocities while the latter takes into account the boundary effects. Radiation and free convection flow through a porous medium using Rosseland approximation for the radiative heat flux was analyzed by Raptis [14]. Chamkha[15] regarded solar radiation assisted free convection in the boundary layer adjacent to a vertical flat plate in a uniform porous medium with a more general Darcy-Forchheimer-Brinkman flow model. Kairi [16] studied the effect of viscous dissipation on natural convection in a non-Darcy porous medium saturated with non-Newtonian fluid of variable viscosity. Murthy [17] examined the combined radiation and mixed convection from a permeable vertical wall in a non-Darcy porous media. The thermal radiation phenomena of non Newtonian fluids over a horizontal plate with variable surface temperature in porous medium was investigated by Mohammadein and El-Amin [18]. Magnetic field effects on convective flows in porous media and thermal radiation have been widely studied [19-33].

Viscous dissipation changes the temperature distributions by playing a role like energy source, which leads to affect heat transfer rates. The effect of viscous dissipation depends on whether the sheet is being cooled or heated. Heat transfer analysis over porous surface is of much practical interest due to its abundant applications. To be more specific, heat-treated materials travelling between a feed roll and wind-up roll or materials manufactured by extrusion, glass-fibre and paper production, cooling of metallic sheets or electronic chips, crystal growing are few practical applications of flow over a stretching sheet [26]. Murthy and Singh [34] studied viscous dissipation on non-Darcy natural convection regime in porous media saturated with Newtonian fluid.

The combined heat and mass transfer problems with chemical reactions are of importance in many processes, and therefore have received a considerable amount of attention in recent years. In processes, such as drying, evaporation at the surface of a water body, energy transfer in a wet cooling tower and the flow in desert cooler, groves of fruit trees, electric power generation; the heat and mass transfer occur simultaneously. In many chemical engineering processes, a chemical reaction between a foreign mass and the fluid does occur. These processes take place in numerous industrial applications, such as the polymer production, the manufacturing of ceramics or glassware, food processing. Randasamy and Palanimani [35] studied on effects of chemical reactions, heat and mass transfer on nonlinear magnetohydrodynamic boundary layer flow over a wedge with a porous medium in the presence of ohmic heating and viscous dissipation. Postelnicu [36] studied the Influence of chemical reaction on heat and mass transfer by natural convection from vertical surfaces in porous media considering Soret and Dufour effects. The flow of nanofluids may also be affected by chemical heating (heat generated in exothermic reactions). Most chemical reactions involve the breaking and formation of chemical bonds. It requires energy to break a chemical bond but energy is released when chemical bonds are formed. The amount of heat generated by a reaction can be quantified. According to Aziz [37], because chemical reactions release or absorb energy, they affect the temperature of their surroundings. Exothermic chemical reactions heat up while endothermic reactions cool down their surroundings.

Most of the studies on flows of nanofluids focus mainly on boundary layer flow and heat transfer of incompressible Newtonian fluids. Now a days, since the increasing demand of nanofluids in science and technology is growing alarmingly, great attention has to be given to convective transport of these fluids. However, heat and mass transfer of nanofluids through a porous medium with effects of thermal radiation, viscous dissipation and chemical

reaction are not adequately studied in a comprehensive way. Thus, to the best of authors' knowledge, so far the simultaneous effects of these quantities in the presence of magnetic field on heat and mass transfer flow of nanofluids through a porous medium has not been analyzed. Hence, this problem is investigated. The governing boundary layer equations are reduced to a system of non linear ordinary differential equations using similarity transformations and the resulting equations are solved numerically by using the Keller box scheme. A parametric study is conducted to illustrate the influence of various governing parameters on the Velocity, Temperature, Concentration, Skin-Friction Coefficient, Nusselt number and Sherwood number are discussed in detail.

2. FORMULATION OF THE PROBLEM

Consider a steady two dimensional laminar boundary layer flow of an incompressible nanofluid over a stretching sheet. It has been considered a Cartesian coordinate system with the origin fixed in such a way that the x-axis is taken along the direction of the continuous stretching surface and the y-axis is measured normal to the surface of the sheet. A uniform transverse magnetic field of strength B_0 is applied in the direction of the y-axis. The flow is generated due to the continual stretching of the sheet, caused by the simultaneous application of two equal and opposite forces along the $x-$axis to keep the origin fixed. It is assumed that the induced magnetic field, the external electric field and the electric field due to the polarization of charges are negligible in comparison to the applied magnetic field. In addition to these, the effects of chemical heating, agglomeration and sedimentation of nanoparticles are not included in the study.

The fluid is a water based nanofluid containing two different types of nanoparticles Copper (Cu) and Alumina ($\mathrm{Al_2O_3}$). It is assumed that the base fluid and the nanoparticles are in thermal equilibrium and no slip occurs between them. The thermophysical properties of the nanofluid are given in Table 1 (see Motsumi [38]). The sheet is then stretched with a velocity $\mathrm{U_w(x)}$, varying linearly with the distance from the slit. It is assumed that the surface has temperature T_w and concentrationC_w; the fluid has uniform ambient temperature $\boldsymbol{T_\infty}$ and concentration $\boldsymbol{C_\infty}$. Following these conditions, the governing boundary layer equation of momentum, energy and diffusion with radiation, viscous dissipation and chemical reaction effects of the nanofluids can be written as [8,39,40].

Table 1. Thermophysical properties of water, copper and alumina, motsumi [38]

Physical Quantity	Properties		
	$\boldsymbol{\rho(\mathrm{kg/m^3})}$	$\boldsymbol{C_p}$**(J/kgK)**	**k(W/mK)**
Pure water	997.1	4179	0.613
Cu	8933	385	400
$\mathrm{Al_2O_3}$	3970	765	40

$$\frac{\partial u}{\partial x}+\frac{\partial v}{\partial y}=0 \tag{1}$$

$$u\frac{\partial u}{\partial x}+v\frac{\partial u}{\partial y}=\frac{\boldsymbol{\mu_{nf}}}{\rho_{nf}}\frac{\partial^2 u}{\partial y^2}-\frac{\sigma {B_0}^2}{\rho_{nf}}u-\frac{\boldsymbol{\mu_{nf}}}{\rho_{nf}}\frac{1}{K}u, \tag{2}$$

$$u\frac{\partial T}{\partial x}+v\frac{\partial T}{\partial y}=\alpha_{nf}\frac{\partial^2 T}{\partial y^2}-\frac{1}{(\rho C_p)_{nf}}\frac{\partial q_r}{\partial y}+\frac{\mu_{nf}}{(\rho C_p)_{nf}}\left(\frac{\partial u}{\partial y}\right)^2 \tag{3}$$

$$u\frac{\partial C}{\partial x}+v\frac{\partial C}{\partial y}=D\frac{\partial^2 C}{\partial y^2}+D_1\frac{\partial^2 T}{\partial y^2}-K_0(C-C_\infty) \tag{4}$$

where (u, v) are velocities in the direction of x and y axes, respectively; T is temperature, C is concentration of the nanofluid, q_r is the radiative heat flux, D is species diffusivity, D_1 is the coefficient contribution of mass flux through temperature gradient, K is the permeability of the porous medium, K_0 is the **c**hemical reaction parameter and σ is electrical conductivity.

The dynamic viscosity μ_{nf}, effective density ρ_{nf}**,** thermal diffusivity α_{nf} and heat capacitance $(\rho C_p)_{nf}$ of the nanofluids are given by [8].

$$\begin{cases} \mu_{nf} = \frac{\mu_f}{(1-\emptyset)^{2.5}} \\ \rho_{nf} = (1-\emptyset)\rho_f + \emptyset\rho_s \\ \alpha_{nf} = \frac{k_{nf}}{(\rho C_p)_{nf}} \\ (\rho C_p)_{nf} = (1-\emptyset)(\rho C_p)_f + \emptyset(\rho C_p)_s \end{cases} \tag{5}$$

The thermal conductivity of nanofluids restricted to spherical nanoparticles is approximated by the Maxwell-Garnett model [41] and Guerin et al. [42]

$$k_{nf} = k_f \left(\frac{k_s + 2k_f - 2\emptyset(k_f - k_s)}{k_s + 2k_f + \emptyset(k_f - k_s)} \right) \tag{6}$$

The subscripts f and s refer to the subscripts of quantities in the base fluid and nanoparticle respectively.

The boundary conditions associated to the differential equations are:

$$u = U_w = bx,\ v = 0,\ T = T_w = T_\infty + A\left(\frac{x}{l}\right)^2,\ C = C_w = C_\infty + B\left(\frac{x}{l}\right)^2 \ \text{ at } \ y = 0,$$
$$u \to 0,\ T \to T_\infty,\ C \to C_\infty \ \text{ as } y \to \infty \tag{7}$$

provided that A, B and b are constants, $b > 0$ and l is the characteristic length. According to the Rosseland diffusion approximation Hossain [43] and following Raptis [18], the radiative heat flux q_r is given by

$$q_r = -\frac{4\sigma^*}{3k^*}\frac{\partial T^4}{\partial y}, \tag{8}$$

where σ^* and k^* are the *Stefan-Boltzmann* constant and the *Rosseland mean absorption coefficient*, respectively. We assume that the temperature differences within the flow are sufficiently small such that T^4 may be expressed as a linear function of temperature.

$$T^4 \approx 4T_\infty^3 T - 3T_\infty^4. \tag{9}$$

Using (8) and (9) in equation (3), we obtain

$$\frac{\partial q_r}{\partial y} = -\frac{16\sigma^* T_\infty^3}{3k^*}\frac{\partial^2 T}{\partial y^2}. \tag{10}$$

Let we introduce a stream function $\psi(x, y)$ in the flow field such that

$$u = \frac{\partial \psi}{\partial y}, \quad v = -\frac{\partial \psi}{\partial x}. \tag{11}$$

It is obvious that the continuity equation (1) is satisfied. Using the similarity transformations,

$$\begin{cases} u = bxf'(\eta), \quad v = -(bv_f)^{\frac{1}{2}} f(\eta), \\ T = T_\infty + (T_w - T_\infty) g(\eta), \\ C = C_\infty + (C_w - C_\infty) h(\eta), \\ \eta = \left(\frac{b}{v_f}\right)^{1/2} y, \quad \psi = (bv_f)^{\frac{1}{2}} x f(\eta). \end{cases} \tag{12}$$

On using equations (5), (6) and (10) to equations (2, 3, 4, 7) transform the governing boundary value problem in to couples of ODEs:

$$f''' + \phi_1 \left(f f'' - f'^2 - \frac{M}{\phi_2} f' \right) - K_1 f' = 0, \tag{13}$$

$$\left(1 + \frac{4R}{3}\right) g'' + Pr \phi_3 \frac{k_f}{k_{nf}} \left(f g' - 2 f' g + \frac{Ec}{\phi_4} f''^2 \right) = 0, \tag{14}$$

$$h'' - Sc(2f'h - fh' + \gamma h) + Srg'' = 0, \tag{15}$$

where η is the similarity variable, f is the dimensionless stream function, g dimensionless temperature and h is dimensionless nanoparticles concentration.

The corresponding boundary conditions become:

$$\begin{gathered} f(0) = 0, \ f'(0) = 1, \ g(0) = 1, \ h(0) = 1, \\ f'(\eta) \to 0, \ g(\eta) \to 0, \ h(\eta) \to 0, \text{ as } \eta \to \infty. \end{gathered} \tag{16}$$

Primes denote differentiation with respect to η, $Pr = \frac{v_f}{\alpha_f}$ (Prandtl number), $\gamma = \frac{K_0}{b}$ (Scaled chemical reaction parameter), $K_1 = \frac{v_f}{bK}$ (Porous medium parameter), $M = \frac{\sigma {B_0}^2}{b\rho_f}$ (Magnetic parameter), $Sr = \frac{D_1}{D} \frac{(T_w - T_\infty)}{(C_w - C_\infty)}$ (Soret number), $Sc = \frac{\nu}{D}$ (Schmidt number), $R = \frac{4\sigma^* T_\infty^3}{k^* k_{nf}}$ (Radiation parameter), $Ec = \frac{{u_w}^2}{(C_p)_f (T_w - T_\infty)}$ (Eckert number) and

$$\begin{gathered} \emptyset_1 = (1 - \emptyset)^{2.5} \left[1 - \emptyset + \emptyset \left(\frac{\rho_s}{\rho_f} \right) \right], \ \emptyset_2 = 1 - \emptyset + \emptyset \left(\frac{\rho_s}{\rho_f} \right), \quad \emptyset_3 = 1 - \emptyset + \emptyset \frac{(\rho C_p)_s}{(\rho C_p)_f}, \\ \emptyset_4 = (1 - \emptyset)^{2.5} \left[1 - \emptyset + \emptyset \frac{(\rho C_p)_s}{(\rho C_p)_f} \right]. \end{gathered} \tag{17}$$

The quantities of engineering interest are the *skin-friction coefficient* C_f, the *local Nusselt number* Nu_x and the *local Sherwood number* Sh_x.These parameters respectively characterize the surface drag, wall heat and mass transfer rates. The quantities are defined as:

$$C_f = \frac{2\tau_w}{\rho_f u_w^2}, \qquad Nu_x = \frac{x q_w}{k_f ((T_w - T_\infty)}, \qquad Sh_x = \frac{x J_w}{D((C_w - C_\infty)}. \tag{18}$$

where τ_w, q_w and J_w are the *shear stress*, *heat flux* and *mass flux* at the surface, respectively and are defined by

$$\tau_w = -\mu_{nf} \left(\frac{\partial u}{\partial y} \right)_{y=0}, \quad q_w = -\left(k_{nf} + \frac{16\sigma^* T_\infty^3}{3k^*} \right) \left(\frac{\partial T}{\partial y} \right)_{y=0}, \quad J_w = -D \left(\frac{\partial C}{\partial y} \right)_{y=0}. \tag{19}$$

Using (18) and (19), the *dimensionless skin friction coefficient (surface drag)*, *wall heat* and *mass transfer rates* become:

$$C_f(1-\emptyset)^{2.5}\sqrt{Re_x} = -2f''(0) \quad , \quad \frac{Nu_x}{\sqrt{Re_x}}\frac{k_f}{k_{nf}} = -\left(1+\frac{4R}{3}\right)g'(0) \text{ and } \frac{Sh_x}{\sqrt{Re_x}} = -h'(0), \tag{20}$$

where $Re_x = \frac{xu_w}{v_f}$ is the local Reynolds number.

3. NUMERICAL SOLUTION

Since equations 13-15 are highly non-linear, it is difficult to find the closed form solutions. Thus, the solutions of these equations with the boundary conditions (16) are solved numerically using the Keller box method. The accuracy of the method depends on the choice of the initial guesses. The following initial guesses are chosen:

$$f_0(\eta) = 1 - e^{-\eta} \ , \quad g_0(\eta) = e^{-\eta} \ , \quad h_0(\eta) = e^{-\eta} \ . \tag{21}$$

The choices of the initial guesses depend on the convergence criteria and the boundary conditions (16). The value of the wall shear stress $-f''(0)$ is commonly used as a convergence criterion because in the boundary layer flow calculations the greatest error appears in the wall shear stress parameter as it is explained in Cebeci and Pradshaw [44]. Thus, we used this convergence criterion in the present study. A uniform grid of size 0.01 is chosen to satisfy the convergence criteria of 10^{-7} in our study, which gives about six decimal places accurate to most of the prescribed quantities.

4. RESULTS AND DISCUSSION

In the numerical solutions, the effects of viscous dissipation, thermal radiation and chemical reaction on heat and mass transfer characteristics through a porous media of nanofluid were considered. Two types of nanoparticles, namely, Copper and Alumina, with water as the base fluid with a constant Prandtl number $Pr = 6.2$ were considered. The transformed nonlinear ordinary differential equations (13)-(15) subject to the boundary conditions (16) were solved numerically using the Keller box method as described in Cebeci and Bradshaw [44]. Velocity, temperature and concentration profiles were obtained and we applied the results to compute the skin friction coefficient, the local Nusselt number and local Sherwood number in Equ(18). The numerical results were discussed for the various values of the parameters graphically and in tabular form. To validate the accuracy of the numerical results, comparisons were made with previously published journals by Yohannes and Shankar [39], Kameswaran [8] and Hamad [33] in the absence of thermal radiation, magnetic field and chemical reaction. As shown in Table 2 and Table 3, the results are in nice agreement.

The skin friction coefficients for different values of nanoparticle volume fraction ∅ and when $Pr = 6.2, Ec = 0, Sc = 1.0,\ R = 0,\ Sr = 0.2,\ K_1 = 0$ and $\gamma = 0.08$ are given in Table 2. It is observed that increasing the values of M results in an increase in the skin friction coefficient. The calculated values show good agreements with Hamad [33] and Yohannes and Shankar [39].

Table 2. Comparison of $-\mathbf{f}''(\mathbf{0})$ for various values of M and ∅ when $\mathbf{Pr} = \mathbf{6.2}, \mathbf{Ec} = \mathbf{0}$, $\boldsymbol{Sc} = \mathbf{1.0}$, $\mathbf{K_1} = \mathbf{0}$, $\mathbf{R} = \mathbf{0}$, $\mathbf{Sr} = \mathbf{0.2}$ and, $\boldsymbol{\gamma} = \mathbf{0.08}$

		$-f''(0)$		$-f''(0)$		$-f''(0)$	
M	∅	**Hamad [33]**		**Yohannes and Shankar [39]**		**Present work**	
		Cu	Al_2O_3	**Cu**	Al_2O_3	**Cu**	Al_2O_3
	0.05	1.10892	1.00538	1.1089	--------	1.108923	1.005385
0	0.1	1.17475	0.99877	1.1747	--------	1.174748	0.998781
	0.15	1.20886	0.98185	1.2089	--------	1.208864	0.981854
	0.2	1.21804	0.95592	1.2180	--------	1.218045	0.955931
	0.05	1.29210	1.20441	1.2921	--------	1.292102	1.204412
0.5	0.1	1.32825	1.17548	1.3282	--------	1.328249	1.175484
	0.15	1.33955	1.13889	1.3396	--------	1.339554	1.138892
	0.2	1.33036	1.09544	1.3304	--------	1.330356	1.095444
	0.05	1.45236	1.37493	1.4524	--------	1.452361	1.374930
	0.1	1.46576	1.32890	1.4658	--------	1.465763	1.328901
1	0.15	1.45858	1.27677	1.4586	--------	1.458582	1.276766
	0.2	1.43390	1.21910	1.4339	--------	1.433898	1.219104
2	0.05	1.72887	1.66436	1.7289	--------	1.728872	1.664356
	0.1	1.70789	1.59198	1.7079	--------	1.707892	1.591984
	0.15	1.67140	1.51534	1.6714	--------	1.671398	1.515336
	0.2	1.62126	1.43480	1.6213	--------	1.621264	1.434799

The heat transfer coefficients are shown in Table 3 for different values of Prandtl numbers. In this case, we took $\emptyset = R = M = Ec = 0$. As it is shown in the table the heat transfer coefficient increases with an increase of Prandtl number. This is true because by definition, Prandtl number is the ratio of kinematic viscosity to thermal diffusivity. An increase in the values of Prandtl number implies that momentum diffusivity dominates thermal diffusivity. Hence, the rate of heat transfer at the surface increases with increasing values of Prandtl number. The present results are in good agreement with the earlier findings by Yohannes [37] and Kameswaran [8].

Table 3. Comparison of the values of wall temperature gradient $-\mathbf{g}'(\mathbf{0})$ for different values of Prandtl numbers Pr when ∅=R=M=K_1=Ec=0

Pr	**0.72**	**1**	**3**	**10**	**100**
Kameswaran [8]	1.08852	1.33333	2.50973	4.79687	15.71163
Yohannes and Shankar [39]	1.0886	1.3333	2.5097	4.7970	15.7198
Present study	1.088621	1.333332	2.509727	4.797002	15.719830

Let us see the effects of viscous dissipation parameter, thermal radiation parameter, scaled chemical reaction parameter, Soret number, Schmidt number, Prandtl number and magnetic parameter on various fluid dynamic quantities as presented graphically. Unless otherwise mentioned, the default values are *Pr =6.2, M =0.5,*$Ec = 1$*,* $\emptyset = 0.1$*,* $Sc = 1$*,* γ *= 0.08,* $Sr = 0.2$**,** $R = 2$ and $K_1 = 1$ for our subsequent results.

Figs. 1-3 illustrate the effects of the nanoparticle volume fraction ∅ on the velocity, temperature and concentration profiles in the case of both nanofluids. As the nanoparticle volume fraction increases, the Cu -water nanofluid velocity decreases while the Al_2O_3 –

water nanofluid velocity increases. As it is shown in Fig. 2, the increment of volume fraction of nanoparticles increases the thermal conductivity of the nanofluid and in turn results a thickening of the thermal boundary layer. It is also observed that the temperature distribution in a Cu–water nanofluid is higher than that of Al_2O_3–water nanofluid; this is an anticipated result because Cu is good conductor of heat and electricity. The Al_2O_3-water nanofluid concentration decreases as the nanoparticle volume fraction of it increases. But the contrary is true to that of Cu -water nanofluid as shown in Fig. 3.

Fig. 4 illustrates the effect of porous medium parameter K_1 on velocity in the case of Cu-water and Al_2O_3-water nanofluids. When the porous medium parameter increases, the velocity profiles of both nanofluids decrease. As it is observed from the figure, the velocity profile of Al_2O_3–water nanofluid is higher than that of Cu –water nanofluid.

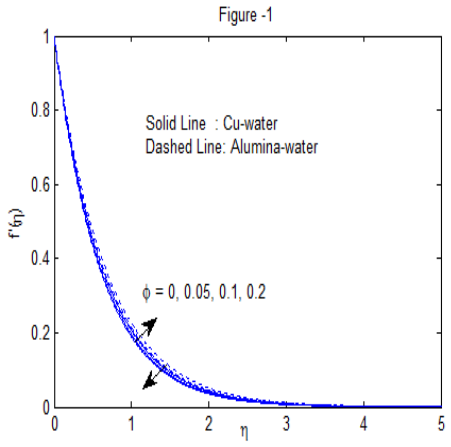

Fig. 1. Effects of ∅ on velocity profile

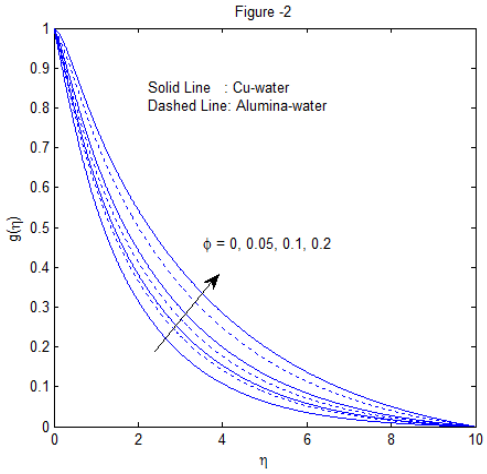

Fig. 2. Effects of ∅ on temperature

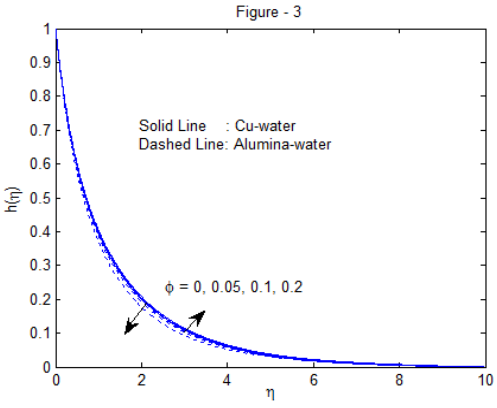

Fig. 3. Effects of ∅ on concentration profile

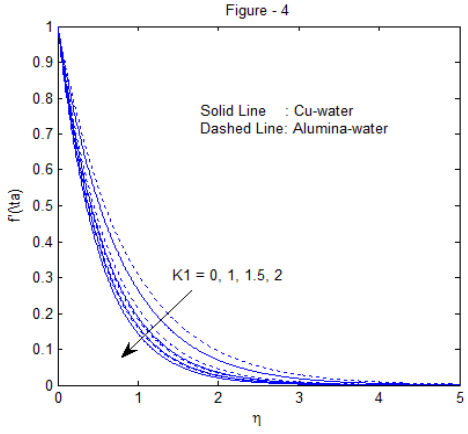

Fig. 4. Effects of K_1 on velocity profile

Fig. 5 illustrates the effect of magnetic parameter M on velocity in the case of Cu-water and Al_2O_3-water nanofluids. When the magnetic parameter increases, the velocity profiles of both nanofluids decrease. This is because the application of transverse magnetic field in an electrically conducting fluid produces a retarding Lorenz force. The force slows down the

motion of the fluid in the boundary layer and hence reduces velocity at the expense of increasing its temperature and the solute concentration. But the solute concentration of Alumina water nanofluid is against this fact as shown in Fig. 3. As it is seen from Fig. 5, the velocity profile of Al_2O_3–water nanofluid is higher than that of Cu –water nanofluid.

Fig. 6 shows the effect of viscous dissipation parameter Ec on temperature profile in the case of both nanofluids. As Ec increases, the temperature profiles of both nanofluids also increase; from Fig. 6, we notice that the effect of an increase in the Eckert number Ec is to increase the temperature distribution. This is in conformity with the fact that the energy is stored in the fluid region as a consequence of dissipation due to viscosity and elastic deformation. It is observed that the temperature increment of Cu-water is more than that of Al_2O_3–water.

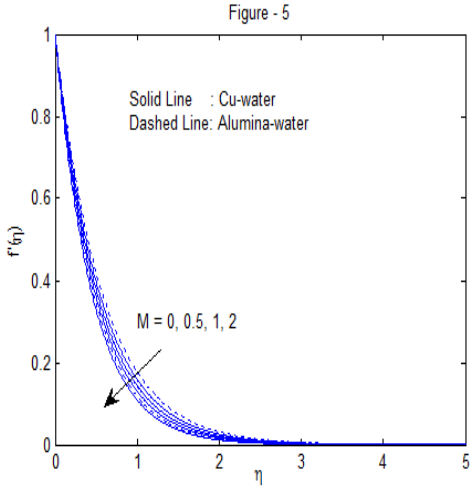

Fig. 5. Effects of M on velocity profile

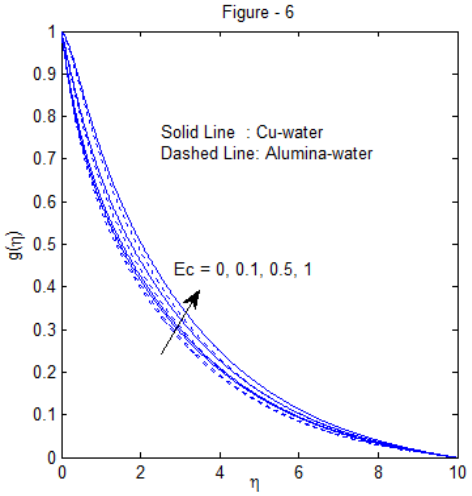

Fig. 6. Effects of Ec on temperature profile

Fig. 7 shows the effect of thermal radiation parameter R on temperature in the case of both nanofluids. As R increases, the temperature profile of both nanofluids also increase; we observed that the temperature increment of Cu -water is more than that of Al_2O_3 –water. The radiation parameter R is responsible to thickening the thermal boundary layer. This enables the nanofluid to release the heat energy from the flow region and causes the system to cool. This is true because increasing the Rosseland approximation results in an increase in temperature.

Fig. 8 illustrates the effect of Schmidt number Sc on concentration profiles in the case of Cu-water and Al_2O_3 -water nanofluids. As the Schmidt number increases, the concentration profiles of both nanofluids decrease. We observed that the concentration increment of Cu -water is more than that of Al_2O_3 –water.

Fig. 9 illustrates the effect of Scaled chemical reaction parameter $\boldsymbol{\gamma}$ on concentration in the case of Cu-water and Al_2O_3-water nanofluids. It is observed that the concentration profile decreases with the increase of chemical reaction parameter whereas its effect shows no substantial changes on velocity and temperature profiles. It is observed that the concentration of Cu -water is more than that of Al_2O_3 –water.

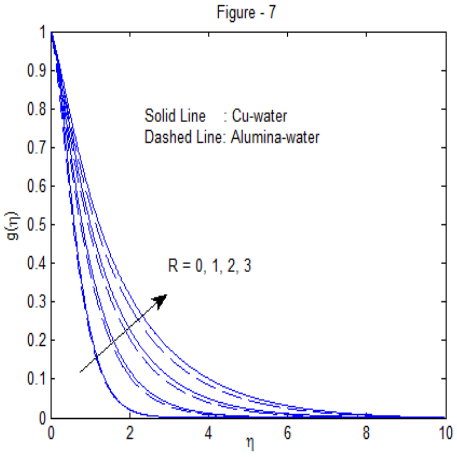

Fig. 7. Effects of R on temperature profile

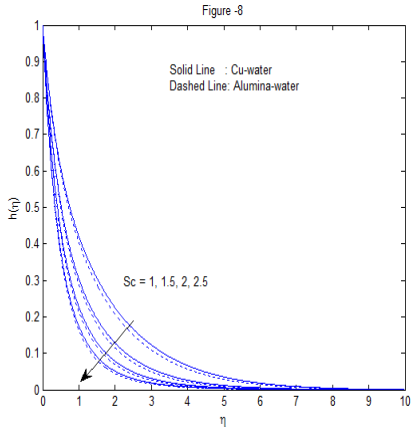

Fig. 8. Effects of Sc on concentration profile

Fig. 10 illustrates the effect of the Soret number Sr on concentration profile in the case of Cu-water and Al_2O_3 water nanofluids. As the Soret number increases, the concentration boundary layer thickness of both nanofluids also increase. It is observed that the concentration increment of Cu –water is more than that of Al_2O_3 –water nanofluid.

We note from Eqs. (14) and (15) that the functions g and h are partially decoupled, hence the chemical reaction parameter γ, Schmidt number Sc and the Soret number Sr have no influence on heat transport. Due to this reason, we have shown the variation of the wall mass transfer rate against γ, Sc and Sr as shown in Table 4. In the case of Cu–water nanofluids it is observed that $-h'(0)$ is an increasing function of Soret number, Schmidt number and chemical reaction parameter. On the other hand, $-h'(0)$ of Al_2O_3-water nanofluid is an increasing function of both Schmidt number and chemical reaction parameter whereas it is a decreasing function of Soret number. It is shown that the Al_2O_3–water nanofluid exhibits higher mass transfer rates as compared to Cu–water nanofluid.

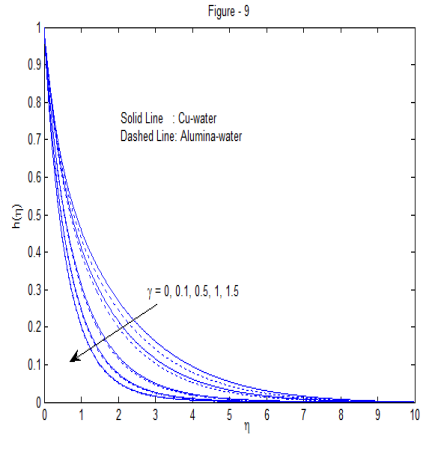

Fig. 9. Effects of γ on concentration profile

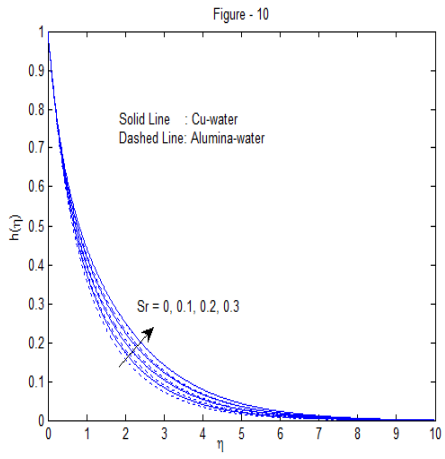

Fig. 10. Effects of Sr on Concentration profile

Fig. 11 shows the skin friction coefficient $-f''(0)$ as a function of the nanoparticle volume fraction $\emptyset$. The skin friction coefficient of Cu-nanofluid increases continuously with increasing values of $\emptyset$ to a maximum value and eventually starts to decline as $\emptyset$ gets larger. On the other hand, the skin friction coefficient for Al_2O_3-water nanofluid decreases as the nanoparticle volume fraction increases. Fig. 12 shows heat transfer coefficient $-g'(0)$ as a function of the nanoparticle volume fraction $\emptyset$. The presence of nanoparticles tends to reduce the wall heat transfer rate. $-g'(0)$ of Cu-water nanofluid declines linearly while that of Al_2O_3 declines very fast for larger values of $\emptyset$.

Table 4. Comparison of the values of skin friction coefficient $-\mathbf{f}''(\mathbf{0})$, wall temperature gradient $-\mathbf{g}'(\mathbf{0})$ and mass transfer rate $-\mathbf{h}'(\mathbf{0})$ for different values of Soret number Sr, Schmidt number Sc and scaled chemical reaction parameter γ

Sr	Cu-water			Al_2O_3-water		
	$\emptyset = 0.1,\ Ec = 1,\ M = 0.5,\ Sc = 1, R = 2,\ \gamma = 0.08,\ Pr = 6.2,\ K_1 = 1$					
	$-f''(0)$	$-g'(0)$	$-h'(0)$	$-f''(0)$	$-g'(0)$	$-h'(0)$
0	1.662602	0.272617	1.202751	1.543296	0.397251	1.231680
0.1	1.662602	0.272617	1.203155	1.543296	0.397251	1.222683
0.2	1.662602	0.272617	1.203559	1.543296	0.397251	1.213685
0.3	1.662602	0.272617	1.203963	1.543296	0.397251	1.204688
Sc	$\emptyset = 0.1,\ M = 0.5,\ Ec = 1,\ Sr = 0.2,\ R = 2,\ \gamma = 0.08,\ Pr = 6.2,\ K_1 = 1$					
1	1.662602	0.272617	1.203559	1.543296	0.397251	1.213685
1.5	1.662602	0.272617	1.573745	1.543296	0.397251	1.586397
2	1.662602	0.272617	1.886822	1.543296	0.397251	1.900611
2.5	1.662602	0.272617	2.162307	1.543296	0.397251	2.176723
γ	$\emptyset = 0.1, Ec = 1, R = 2,$		$Sc = 1, M = 0.5,$		$Sr = 0.2, Pr = 6.2,\ K_1 = 1$	
0	1.662602	0.272617	1.139639	1.543296	0.397251	1.154748
0.1	1.662602	0.272617	1.217724	1.543296	0.397251	1.226969
0.5	1.662602	0.272617	1.437431	1.543296	0.397251	1.438171
1	1.662602	0.272617	1.641639	1.543296	0.397251	1.638450

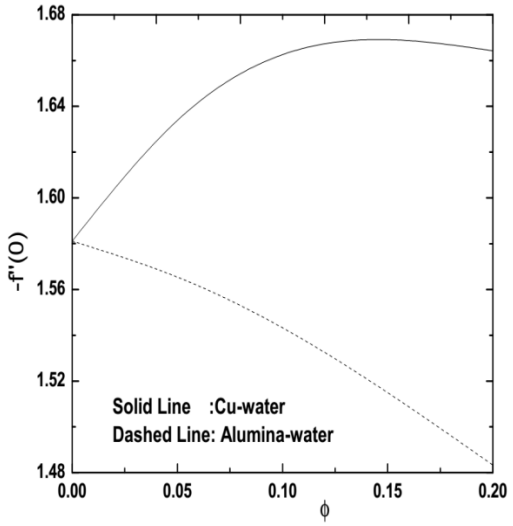

Fig. 11. Effects of ∅ on skin friction coefficient

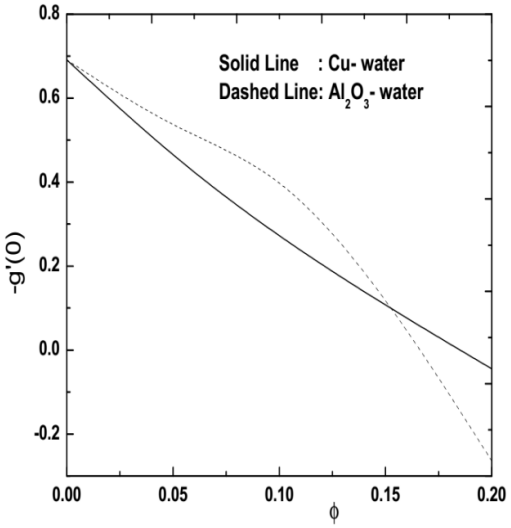

Fig. 12. Effects of ∅ on heat transfer coefficient

Fig. 13 shows the dimensionless wall mass transfer rate $-h'(0)$ as a function of the nanoparticle volume fraction ∅. It is observed that $-h'(0)$ is an increasing function of ∅ for both nanofluids. The Al_2O_3–water nanofluid exhibits higher wall mass transfer rate as compared to Cu–water nanofluid. The presence of nanoparticles tends to increase the wall mass transfer rate.

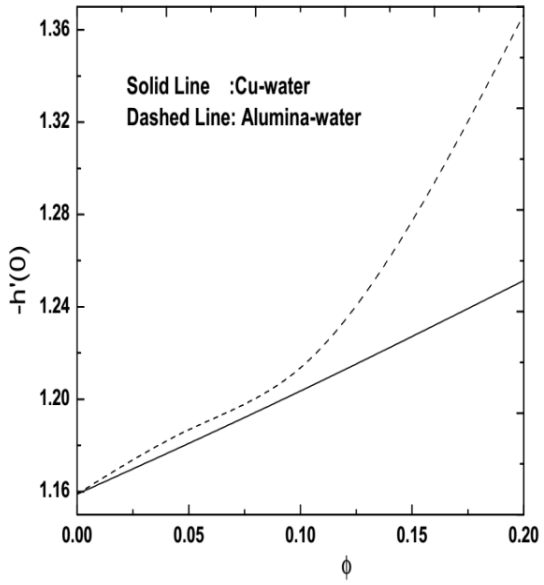

Fig. 13. Effects of ∅ on mass transfer coefficient

Fig. 14 and Fig. 15 show the wall heat transfer rate $-g'(0)$ and the wall mass transfer rate $-h'(0)$ respectively, as functions of the viscous dissipation parameter Ec for different values of the magnetic parameter M. It is observed that $-g'(0)$ is a decreasing function of both Ec and M while $-h'(0)$ is an increasing function of Ec and a decreasing function of M. This is due to the fact that the transverse magnetic field contributes to the thickening of the thermal boundary layer. This in turn results in lowering the heat transfer rate. Consequently, the warmer the boundary layer the more the nanofluid diffuses, which brings about a rise in the nanoparticle volume fraction ∅. This causes the thermal concentration rate to decrease. On the other hand, an increment in the solid volume fraction ∅ and the Eckert number Ec yields an increment in the nanofluid's temperature; this leads to a rapid decline in the heat transfer rates. The Al_2O_3–water nanofluid exhibits higher wall heat and mass transfer rates as compared to Cu–water nanofluid.

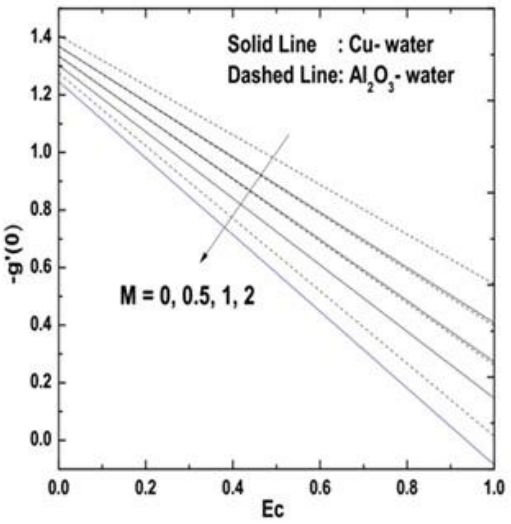

Fig. 14. Effects of M and Ec on heat transfer coefficient

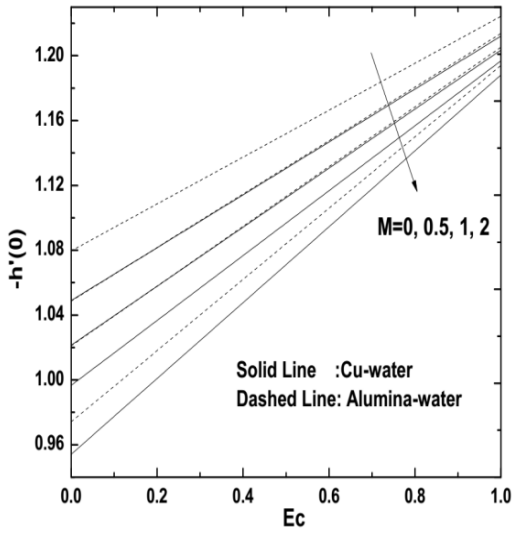

Fig. 15. Effects of M and Ec on mass transfer coeff.

The effect of porous media and thermal radiation on wall heat transfer rate is shown in Fig.16 in the case of Cu–water and Al_2O_3–water nanofluids. The influence of porous media is to reduce the wall heat transfer rate. The Al_2O_3–water nanofluid exhibits higher wall heat transfer rate as compared to Cu–water nanofluid.

The effect of thermal radiation and viscous dissipation on the wall heat transfer rate is shown in Fig.17 in the case of Cu–water and Al_2O_3–water nanofluids. The influence of viscous dissipation is to reduce the wall heat transfer rate. For smaller values of

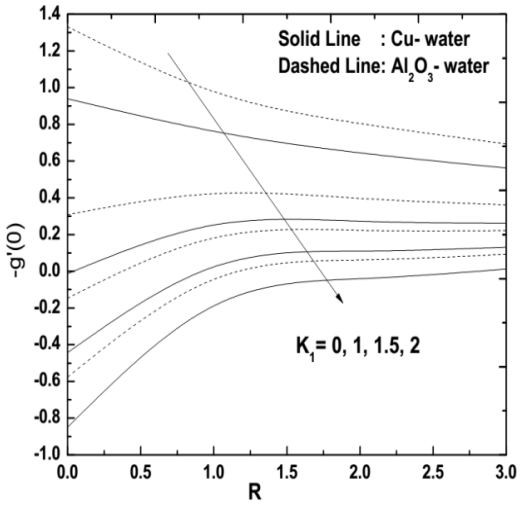

Fig. 16. Effects of R and K_1 on mass transfer coeff.

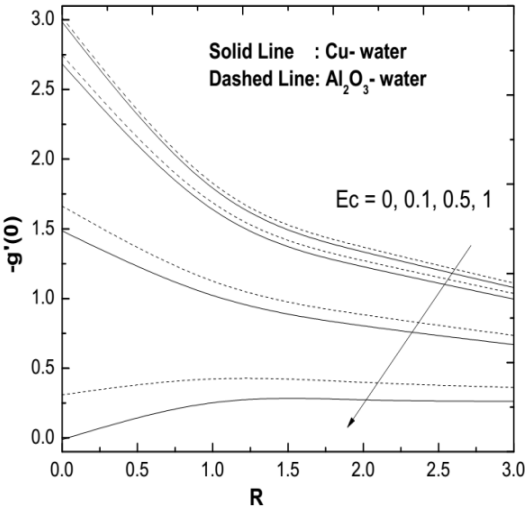

Fig. 17. Effects of R and Ec on heat Transfer Coefficient

Eckert number, thermal radiation reduces heat transfer rate faster but it enhances for larger values of Eckert number as shown in Fig.17. The cumulative effect of the thermal radiation and viscous dissipation is to reduce the wall heat transfer rate. It is fact to mention that the radiation parameter R favours the nanofluids for the thickening of the thermal boundary layer which releases heat energy from the flow region and causes the cooling of the system. And it is also true because temperature increases by increasing the Rosseland approximation; which leads to a decline in the heat transfer rates. It is investigated that Al_2O_3-water nanofluid exhibits higher wall heat transfer rate compared to that of Cu-water nanofluid.

The effect of magnetic field on skin friction coefficient, wall heat and mass transfer rates are shown in Fig. 18(a) in the case of Cu–water and Al_2O_3–water nanofluids. Skin friction coefficient increases with magnetic parameter while a magnetic field is to reduce both the wall heat and mass transfer rates. It is investigated that Al_2O_3-water nanofluid exhibits higher wall heat and mass transfer rates compared to that of Cu-water. But it is found that the Cu-water nanofluid exhibits higher skin friction coefficient than that of Al_2O_3.

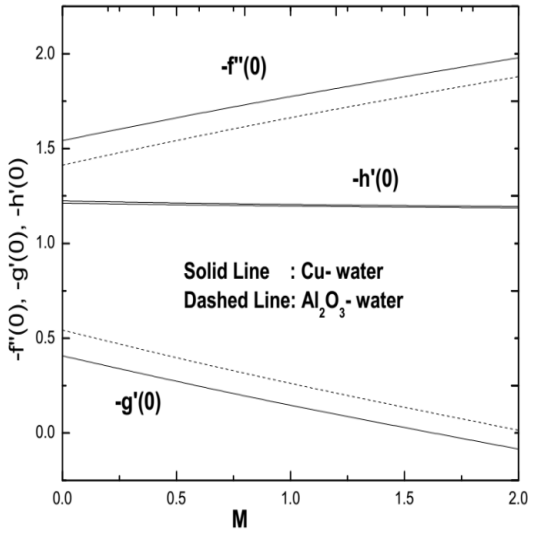

Fig. 18. (a) Effects of M

The effect of porous media on skin friction coefficient, wall heat and mass transfer rates are shown in Fig. 18(b) in the case of Cu–water and Al_2O_3–water nanofluids. Skin friction coefficient increases with porous medium parameter while porous media is to reduce both the wall heat and mass transfer rates (although the effect of K_1 on mass transfer rate is not obviously seen). It is investigated that Al_2O_3-water nanofluid exhibits higher wall heat and mass transfer rates compared to that of Cu-water. But it is found that the Cu-water nanofluid exhibits higher skin friction coefficient compared to that of Al_2O_3.

The effect of thermal radiation on skin friction coefficient, wall heat and mass transfer rates are shown in Fig. 18(c) in the case of Cu–water and Al_2O_3–water nanofluids. It is observed that radiation parameter has no effect on skin friction coefficient whereas it is to reduce the wall mass transfer rate. It is investigated that Al_2O_3-water nanofluid exhibits higher wall mass transfer rate compared to that of Cu-water for larger values of R. It is also observed

that the heat transfer rate increases for smaller values of R but remains constant for larger values R (This statement is obviously supplemented by Fig. 16).

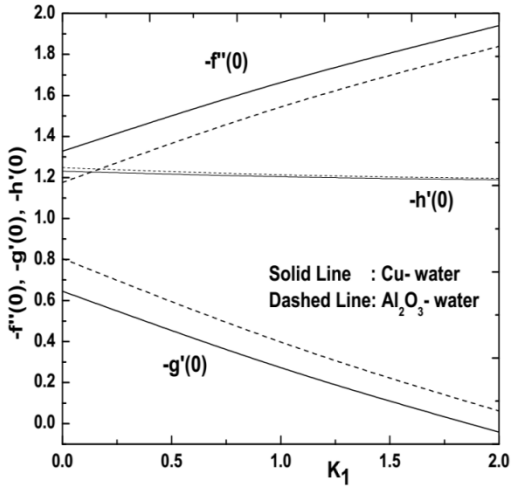

Fig. 18. (b) Effects of K_1

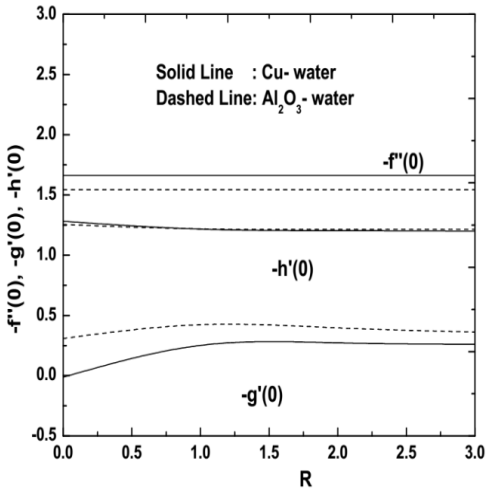

Fig. 18. (c) Effects of R

Fig. 18. Effects of M, K_1 and R on skin friction, heat transfer and mass transfer coefficients

5. CONCLUSION

The problem of boundary layer flow of a nanofluid through a porous medium subjected to a magnetic field, thermal radiation, viscous dissipation and chemical reaction effects has been analyzed for Cu–water and Al_2O_3–water nanofluids. The governing equations associated to the boundary conditions were transformed to a two point non-linear ODEs with the help of similarity transformation equations. The solutions of the problem were numerically solved with the help of the Keller box method. The following results were investigated:

- The velocity profile of both nanofluids decrease with an increase in magnetic and porous medium parameters. An increase in nanoparticle volume fraction results in a decline of the velocity profile of Cu_water nanofluid whereas it enhances the velocity profile of Al_2O_3 -water nanofluid.
- An increase in nanoparticle volume fraction enhances the temperature profile of both nanofluids; but this results in a decline of the concentration of Al_2O_3-water nanofluid and an increase of the concentration of Cu-water nanofluid.
- Viscous dissipation and thermal radiation enhance the temperature profile**.**
- Chemical reaction parameter and Schmidt number reduce the concentration profile but the Soret effect enhances it in the case of both nanofluids.
- Increasing the magnetic parameter results in an increase in the skin friction coefficient where as it decreases the heat and mass transfer rates at the plate surface of both nanofluids.
- The presence of nanoparticle volume fraction, thermal radiation, porous media and viscous dissipation in the flow field is to reduce the rate of thermal boundary layer thickness of both nanofluids.

- The wall mass transfer rate is an increasing function of the Schmidt number, the nanoparticle volume fraction, the viscous dissipation and chemical reaction parameters while the Soret effect reduces the mass transfer rate at the plate surface of both nanofluids.
- In general, the Al_2O_3-water nanofluid shows thicker velocity layer at the plate than Cu-water nanofluids; Al_2O_3-water nanofluid exhibits thicker thermal and concentration boundary layer than that of Cu-water nanofluid; Cu-water nanofluid shows higher skin friction coefficient than Al_2O_3-water nanofluid.

COMPETING INTERESTS

Authors have declared that no competing interests exist.

REFERENCES

1. Ahmadreza AB. Application of nanofluid for heat transfer enhancement. (PID: 2739168),EEE-5425; 2013.
2. Choi SUS. Enhancing thermal conductivity of fluids with nanoparticles, developments and applications of non-Newtonian flows. United States.1995;66:99-105.
3. Mnyusiwalla A, Abdallah SD, Peter AS. Mind the gap: Science and ethics in nanotechnology. Nanotechnology. 2003;14:R9-R13.
4. Buongiorno J. Convective transport in nanofluids. Journal of Heat Transfer (American Society of Mechanical Engineers). 2010;128(3):240-250.
5. Hamada MA, Pop I, Ismail AI. Magnetic field effects on free convection flow of a nanofluid past a vertical semi-infinite flat plate. Nonlinear Analysis: Real World Applications. 2011;12(3):1338–1346.
6. Makinde OD, Aziz A. Boundary layer flow of a nanofluid past a stretching sheet with a convective boundary condition. International Journal of Thermal Sciences. 2011; 50:1326-1332.
7. Ahmad S, Rohni AM and Pop I. Blasius and sakiadis problems in nanofluids. Acta Mechanical. 2011;218:195-204.
8. Kameswaran PK, Narayana M, Sibanda P, Murthy PV. Hydromagnetic nanofluid flow due to a stretching or shrinking sheet with viscous dissipation and chemical reaction effects. International Journal of Heat and Mass Transfer. 2012;55:7587-7595.
9. Khan WA, Pop I. Boundary-layer flow of a nanofluid past a stretching sheet. Int. J. Heat and Mass Transf. 2010;53(11–12):2477–2483.
10. Khan MS, Karim I, Ali LE, Islam A. Unsteady MHD free convection boundary-layer flow of a nanofluid along a stretching sheet with thermal radiation and viscous dissipation effects. Int. Nano Lett. 2012;2:24. doi:10.1186/2228-5326-2-24.
11. Chul JC, Seok PJ, Stephen USC. Electrokinetic effects of charged nanoparticles in microfluidic Couette flow. J. of Colloid and Interface Science. 2011;363:59-63.
12. Weiting J, Guoliang D, Hao P, Haitao H. Modeling of nanoparticles' aggregation and sedimentation in nanofluid. Current Applied Physics. 2010;10(3):934–941.
13. Rami YJ, Fawzi A, Fahmi AAR. Darcy-Forchheimer mixed convection heat and mass transfer in fluid saturated porous media. Int. J. of Num. Meth. for Heat & Fluid Flow. 2001;11(6):600-618.
14. Raptis A. Radiation and free convection flow through a porous medium. Int. Comm. in Heat and Mass Transfer. 1998;25:289-295.
15. Chamkha AJ. Solar radiation assisted convection in uniform porous medium supported by a vertical plate. Transaction ASME J. of Heat Transfer. 1997;119:89-96.

16. Kairi RR. Effect of viscous dissipation on natural convection in a non-Darcy porous medium saturated with non-Newtonian fluid of variable viscosity. The Open Transport Phenomena Journal. 2011;3:1-8.
17. Murthy PV, Mukherjee S, Srinivasacharya D, Krishna PV. Combined radiation and mixed convection from a vertical wall with suction/injection in a non-Darcy porous media. Acta Mechanica. 2004;168:145-156.
18. Mohammadein AA, El-Amin MF. Thermal radiation effect on power law fluid over a Horizontal plate embedded in a porous medium. Int. Comm. in Heat and Mass Transfer. 2000;27:1025-1035.
19. Nield DA, Bejan A. Convection in porous media. Third edition, Springer, New York; 2006
20. Ingham DB, Pop I. Transport phenomena in porous media. Vol. III, Elsevier, Oxford; 2005.
21. Vafai K. Handbook of porous media. Second edition, Taylor & Francis, New York; 2005.
22. Vadasz P. Emerging topics in heat and mass transfer in porous media. Springer, New York; 2008.
23. Michalis Xenos. Radiation effects on flow past a stretching plate with temperature dependent viscosity. Applied Mathematics. 2013;4:1-5.
24. Gnaneswara R. Influence of thermal radiation, viscous dissipation and hall current on MHD convection flow over a stretched vertical flat plate. Ain Shams Engineering Journal. 2014;5:169-175.
25. Hady FM, Ibrahim FS, Abdel-Gaied SM, Mohamed R Eid. Radiation effect on viscous flow of a nanofluid and heat transfer over a nonlinearly stretching sheet. Nanoscale Res. Lett. 2012;7:229.
26. Hadjinicolaou K. Heat transfer in a viscous fluid over a stretching sheet with viscous dissipation and internal heat generation. Int. Commun. Heat Mass Transfer. 1993;20:417-430.
27. Rajesh V. Radiation effects on MHD free convective flow near a vertical plate with ramped wall temperature. Int. J. of Appl. Math. and Mech. 2010;6(21):60-77.
28. Raptis A. Free convective oscillatory flow and mass transfer past a porous plate in the presence of radiation for an optically thin fluid. Thermal Science. 2011;15(3):849-857.
29. Jafar K, Nazar R, Ishak A, Pop I. MHD flow and heat transfer over stretching/shrinking sheets with external magnetic field, viscous dissipation and Joule Effects. Can. J. Chem. Eng. 2011;9999:1-11.
30. Afifi A. MHD free convective flow and mass transfer over a stretching sheet with chemical reaction. Heat Mass Transfer. 2004;40:495-500.
31. Hamada MAA, Pop I, Ismail Al Md. Magnetic field effects on free convection flow of a nanofluid past a vertical semi-infinite flat plate. Nonlinear Analysis: Real World Appl. 2011;12:1338-1346.
32. Chiam TC. Magneto hydrodynamic boundary layer flow due to a continuous moving flat plate. Computers and Mathematics with Applications. 1993;26(4):1-7.
33. Hamad MAA. Analytical solution of natural convection flow of a nanofluid over a linearly stretching sheet in the presence of magnetic field. Int. Commun. Heat Mass Transfer. 2011;38(4):487-492.
34. Murthy PV and Singh P. Effect of viscous dissipation on a non-Darcy natural convection regime. Int. J. of Heat and Mass Transfer. 1997;40:1251-1260.
35. Kandasamy R, Palanimani PG. Effects of chemical reactions, heat, and mass transfer on nonlinear magnetohydrodynamic boundary layer flow over a wedge with a porous medium in the presence of ohmic heating and viscous dissipation. J. Porous Media. 2007;10:489-502.

36. Postelnicu A. Influence of chemical reaction on heat and mass transfer by natural convection from vertical surfaces in porous media considering Soret and Dufour effects. Heat Mass Transfer. 2007;43:595-602.
37. Aziz A, Jashim Uddin Md, Hamad MAA, Ismail AI Md. MHD flow over an inclined radiating plate with the temperature-dependent thermal conductivity, variable reactive index, and heat generation. Heat Transfer—Asian Research. 2012;41(3):241-259.
38. T G Motsumi TG, Makinde OD. Effects of thermal radiation and viscous dissipation on boundary layer flow of nanofluids over a permeable moving flat plate. Phys. Scr. 2012;86:1-8.
39. Yohannes YK , Shankar B. Heat and mass transfer in MHD flow of nanofluids through a porous media due to a stretching sheet with viscous dissipation and chemical reaction effects. Caribian J. of Scie. and Tech. 2013;1:1-17.
40. Hady FM, Mohamed R Eid, Abd-Elsalam MR, Mostafa AA. The Blasius and Sakiadis flow in a nanofluid through a porous medium in the presence of thermal radiation under a convective surface boundary condition. IJEIT. 2013;3(3):225-234.
41. Maxwell Garnett JC. Colours in metal glasses and in metallic films. Philos. Phil. Trans. R. Soc. Lond. 1904;203:385-420.
42. Guerin CA, Mallet P, Sentenac A. Effective-medium theory for finite size aggregates. J. Opt. Soc. Am. 2006;23(2):349-358.
43. Hossain MA, Takhar HS. Radiation effect on mixed convection along a vertical plate with uniform surface temperature. Heat Mass Transf. 1996;31:243-248.
44. Cebeci T, Bradshaw P. Physical and Computational Aspects of Convective Heat Transfer. Springer-Verlag, New York; 1988.

Peer-review history:
The peer review history for this paper can be accessed here:
http://www.sciencedomain.org/review-history.php?iid=528&id=16&aid=5201